



Mapping cortical bone stiffness and mineralization from endosteal to periosteal surfaces of bovine mid-diaphyseal femur

I. S. Hage¹ · R. S. Hage² · R. A. Yassine³ · C. Y. Seif³ · R. F. Hamade³

Received: 22 July 2020 / Accepted: 23 February 2021 / Published online: 6 April 2021
© The Japanese Society Bone and Mineral Research 2021

Abstract

Introduction While bone literature abounds with correlations of mechanical stiffness to mineralization, such correlations are reported without relating the findings to specific intracortical locations. This study reports on mapping of stiffness and mineralization distributions in ring-shaped cortical bone samples sliced from mid-diaphyseal bovine femur. Stiffness and mineralization measurements were conducted at points across the intracortical thickness along radial lines emanating from the inner (endosteal) surface to the outer (periosteal) surface. Measurements were taken along approximately 4 mm distance of cortical bone thickness.

Materials and methods Three experimental techniques were employed: Vickers microhardness (HV), energy-dispersive X-ray (EDX) spectroscopy, and computed tomography (CT). Stiffness values were extracted from the Vickers microhardness tests. Elemental mineralization values (calcium %wt. and phosphorus %wt.) were determined from EDX data. All measurements were repeated on three different femur bones taken from different bovines (collected fresh from butcher).

Results The study plots stiffness values and elemental mineralization (calcium %wt. and phosphorus %wt.) versus cortical thickness. Both stiffness and Ca %wt. and P %wt. are found to track and to linearly increase when plotted along the radial distance. The stiffness and mineralization trends collected from Vickers and EDX measurements were verified by employing the CT number (Hounsfield units, HU) via CT scans of the same bone samples. Data fitting via statistical methods revealed that all correlations were statistically significant.

Conclusion Starting from endosteal to periosteal surfaces of mid-diaphyseal bovine femur, it was found that stiffness, mineralization, and HU values all exhibit increasing and correlating trends.

Keywords Bone · Intracortical · Stiffness · Mineralization · EDX · CT · Statistical correlations

Introduction

Generically speaking, cortical bone stiffness has long been established to be directly proportional to bone mineral content (e.g., Boivin et al. [1], Bala et al. [2], Haider et al. [3],

Cai et al. [4]). Hage and Hamade [5] assessed intracortical stiffness values via microhardness measurements in conjunction with homogenization numerical solutions extracted from intracortical porosity. Mineralization wise, calcium and phosphate atoms are typically present in cortical bone as hydroxyapatite. Smaller amounts of carbon, nitrogen, oxygen, magnesium, sodium, sulfur, and potassium are also found (e.g., Boskey and Posner [6]). Minerals and collagen determine the compact bone mechanical behavior [7, 8] and biomechanical properties [9]. In human calcanei bone, positive linear correlations were found to exist between the degree of mineralization and both the elastic modulus and strength of the bone [10]. Bone strength was reported to increase with increasing mineralization of transiliac bone biopsies in osteoporotic women using alendronate [11]. Hansson et al. [12], correlated ($R=0.86$) bone mineral content and ultimate compressive strength and found that bone

✉ R. F. Hamade
rh13@aub.edu.lb

¹ Department of Mechanical Engineering, Notre Dame University-Louaize, Zouk Mikael, P.O. Box: 72, Zouk Mosbeh, Lebanon

² Department of Mathematics, Notre Dame University-Louaize, Zouk Mikael, P.O. Box: 72, Zouk Mosbeh, Lebanon

³ Department of Mechanical Engineering, American University of Beirut, Riad El-Solh, Beirut 1107 2020, Lebanon

strength increased linearly with increasing amounts of mineral content. In an early study, Romanus [13] reported positive correlations between phosphorus and calcium contents with higher significance observed for the ultimate tensile strength and elastic stiffness of the distal half region of the left femur (of experimental dogs). Zaichick and Tzaphlidou [14] studied the Ca, P, and Ca/P concentrations in human trabecular bone and found that while Ca concentrations are reduced with aging, phosphorus concentrations remain unchanged.

An assessment of bone minerals was performed on cortical bone for different animal species using synchrotron radiation microtomography [15]. Abnormal osteoporotic bones were associated with higher Ca/P gradient and it was concluded that Ca/P ratio depends on bone type. A follow up study [16] using X-ray absorptiometry and computed microtomography concluded that Ca/P ratio better describes bone properties where low values of Ca/P ratio are indicative of bone loss. Mandair and Morris [17] utilized Raman spectroscopy to examine mineral and matrix collagen components relative to mineral crystallinity. Using nanoindentation and micro-CT techniques, Willems et al. [18] correlated tissue mineralization density (TMD) to cortical and cancellous bone stiffness of a mandibular condyle. Through statistical analysis of experimental data, TMD was found to affect cancellous bone stiffness more than cortical bone stiffness.

Starting from CT scans, various works related bone stiffness (isotropic [19]), transversely isotropic [20], and orthotropic [21] to HU values. Cuppone et al. [22] demonstrated that bone stiffness increases linearly with CT number. Schneider et al. [23] found an increasing trend between CT number and bone modulus of elasticity for HU values of – 25 to 3000. Hounsfield unit values were directly related to bone density and elastic constants by several workers including Khan et al. [24], Eberle et al. [25], and Gačnik et al. [26].

While many such studies have correlated bone elasticity to mineralization and CT values, to the authors' best knowledge, no other work reports on relating stiffness to specific intracortical locations within bone geometry. The objective of this work is to locally correlate stiffness values to mineralization in terms of the elemental constituents (mainly calcium and phosphorus) at specific bone locations. Using samples cut from mid-diaphysis femur bovine bones, Vickers microhardness tests are conducted along radial lines emanating from the geometrical center of the bone covering the thickness of the cortical bone (from the interior to the exterior regions). Consequently, longitudinal (E_{11}) elastic stiffness values are extracted from these measurements and plotted as function of cortical thickness. Along the same radial lines, bone mineral compositions are quantified using EDX spectroscopy measurements of calcium (%wt. Ca) and phosphorus (%wt. P) content. Stiffness values and elemental bone mineralization values are then statistically correlated as

function of location within the cortical thickness. The same specimens are also CT scanned and Hounsfield units (HU) are determined. Linear trends of values of stiffness, bone mineral content, and HU values are found versus each other and versus radial location. Statistically verified equations are then developed to correlate the observed linear trends of stiffness values versus mineralization and HU values all as function of cortical thickness. All these trends were found to exhibit strong statistical significance.

One merit of this work is the development of simple equations to estimate femur bone mineralization and stiffness as function of location in the cortical thickness. These findings provide an insight into the mechanical behavior at various locations within the cortical bone. The work demonstrates that bone intracortical stiffness varies significantly from interior to exterior regions. This comprehension of bone properties may prove helpful during surgery procedures that involve placing screws to relocate bones or to close fractures. These equations may act as non-invasive method to check for bone porosity, mineralization, and stiffness at given cortical locations. Furthermore, correlating the CT gray values to stiffness and to corresponding mineral content at localized bone locations may potentially aid to detect localized osteoporotic regions.

Materials and methods

Sample preparation

Three bovine femur bones from different healthy cows (with a similar age of 2 years old) were obtained fresh from a butcher. The animals did not witness any trauma before slaughtering and the bones were retrieved undamaged. Slices were cut from the mid-diaphyseal regions using a band saw while being water lubricated to obtain sections that are 1 cm thick. These bone sections resulted in ring-shaped cortical bone specimens. Bone marrow and blood were removed by washing with brine ice water solution and subsequent refrigeration. The brine water was changed by increasing salinity through the addition of two tablespoons of salt for a period of 24 h. Beyond which, the cut bone samples were allowed to dry.

CT scanning

The ring-shaped sliced specimens were scanned using a Philips Brilliance iCT scanner at the American University of Beirut Medical Center (AUBMC). Scans utilized 256 slices at intervals of 0.67 mm, spaced by 0.33 mm, resulting in voxel size of 0.32 mm³. Scanning was conducted at 0.4 mm/rotation pitch and rotation speed of 0.4/s at voltage and current values of 80 kV and 80 mA, respectively.

The two-dimensional images were saved as DICOM (digital imaging and communication in medicine) files. A total of 1255 slices were passed to MIMICS [27], a commercially available package for segmentation purposes (see Yassine et al. [28] for description of the segmentation process).

Microhardness experiments

On each quadrant of every sliced bone specimen, Vickers microhardness tests (similar to those performed by Hage and Hamade [5]) were performed in accordance with the ASTM E384-11e1 standard at a load of 500 gf and dwell time of 10 s. The surfaces were lightly polished by grinding using silicon carbide (SiC) abrasive paper of progressively finer grit sizes: 600, 800, and 1200 grit. This was followed by polishing with a cloth (2400 grit SiC paper) on a rotary wheel at constant speed and followed by final cleaning. Using a Nexus 4304 microhardness tester, micro-indentation experiments were performed along each radial line of the sliced specimens at approximately 0.5 mm increments. A typical sliced bone specimen is shown in Fig. 1 (top-left) with bone quadrants marked according to the anatomical positions (A: Anterior, P: Posterior, M: Medial, and L: Lateral). Shown

in Fig. 1 (top-right), in each of the four anatomical positions, are marker lines along which Vickers indentations, EDX spectroscopy, and CT scans were performed. Figure 1 (bottom-left) shows a specimen the being mounted on the setup, (bottom-middle) illustrates the internal and external bone regions with respect to the center or origin of the bone, and (bottom-right) is a close-up image showing the micro-indentations.

EDX experiments

Elemental compositions of the cortical specimens was investigated utilizing energy-dispersive X-ray (EDX) analysis (OXFORD EDX detector by TESCAN) operated at 10 kV and a light beam focused at 100 μm . Images were captured using the co-mounted MIRA3 LMU scanning electron microscope (SEM) after applying a thin platinum coating via physical vapor deposition (PVD).

Statistical analysis

Utilizing SPSS[®], a statistical software package from IBM, relationship equations of bone stiffness, mineral content, and

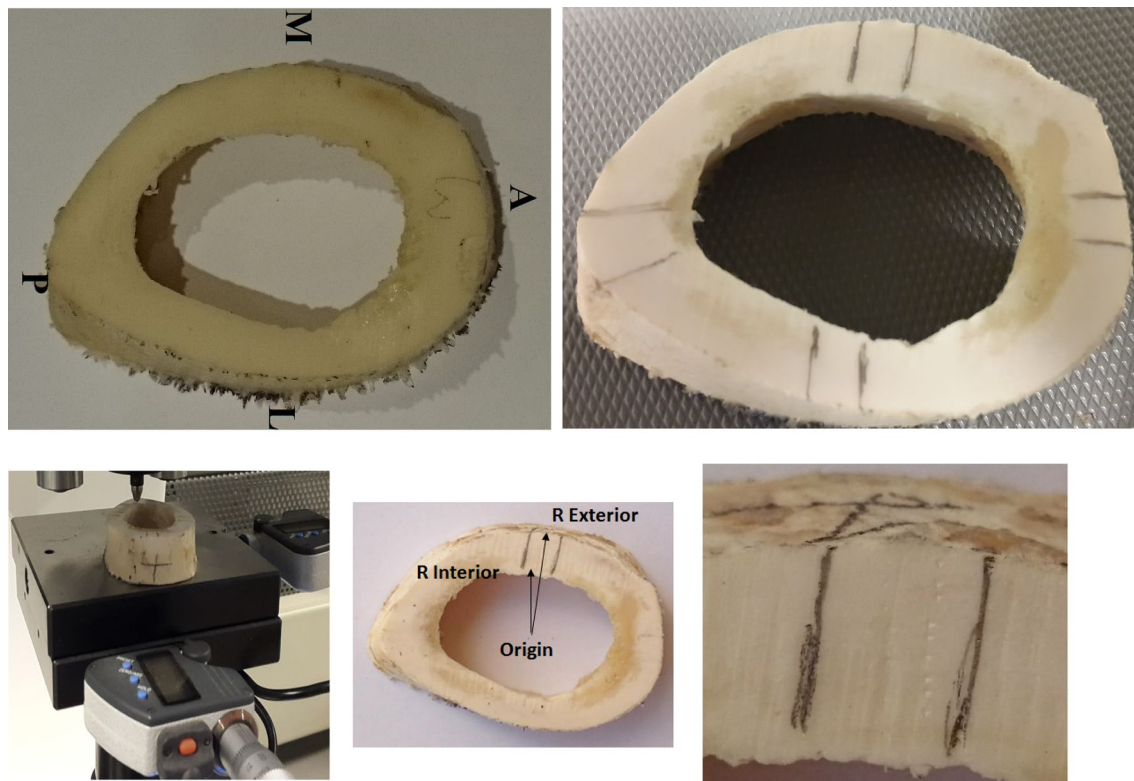


Fig. 1 Typical sliced bone specimen shown: (top-left) marked anatomical positions (A: Anterior, P: Posterior, M: Medial, and L: Lateral), (top-right) with radial lines along which microhardness and EDX measurements are collected, (bottom-left) mounted on the

Nexus 4304 microhardness testing machine, (bottom-middle) with cortical bone center (origin), interior, and exterior radii, and (bottom-right) close-up image of Vickers indentations

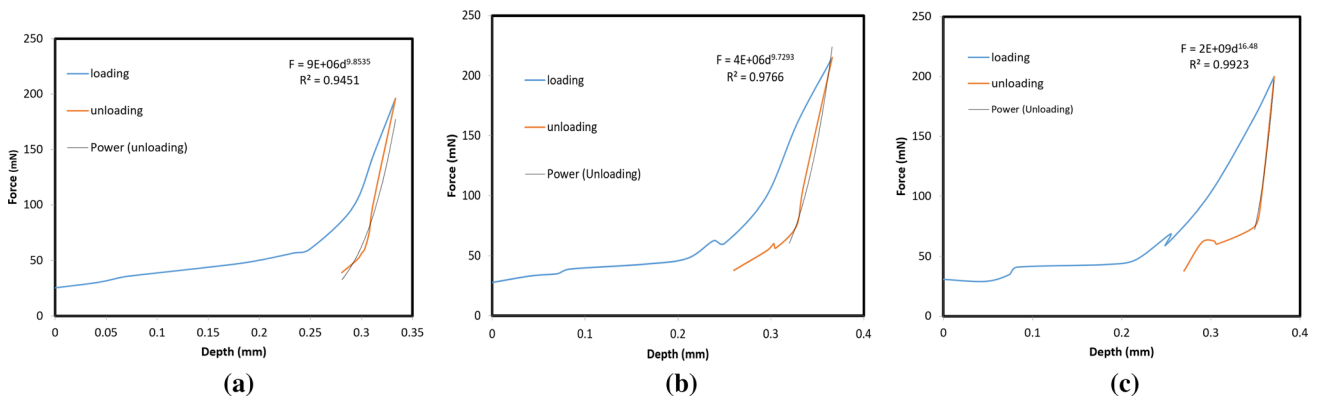


Fig. 2 Three indentation force vs. penetration depth: loading and unloading curves for three bone samples dubbed samples: 1 (a), 2 (b), and 3 (c)

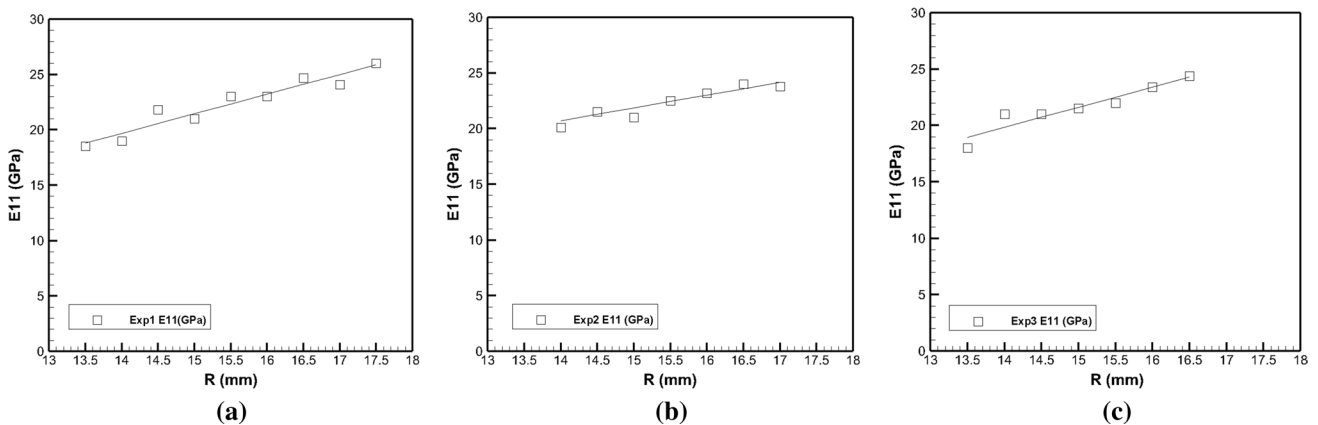


Fig. 3 Longitudinal stiffness modulus E_{11} (GPa) vs. radial distance, R (mm); EXP: experimental results for three samples: 1 (a), 2 (b), and 3 (c)

Table 1 Stiffness modulus, %wt. Ca, and %wt. P versus R: linear trends and their statistical metrics

E_{11} (GPa)	Bone 1	Bone 2	Bone 3	All bones
Equation	$E_{11} = 1.770R - 5.091$	$E_{11} = 1.150R + 4.616$	$E_{11} = 1.786R - 5.171$	$E_{11} = 1.537R - 1.995$
<i>p</i> value	0.00008	0.02	0.001	0.000004
R^2	0.961	0.694	0.895	0.851

CT gray values as function of bone radial distance (thickness), R , were developed using simple and multiple linear regression analysis. This statistical technique allows for developing relationships between two or more variables. Statistical metrics, namely the coefficient of determination, R^2 , p value of the t test, and the F -test (ANOVA), are used to determine the statistical significance of variable variations. Specifically, the percentage of the variation of bone stiffness is explained by the variation in the predictor variables namely bone mineralization and HU value. All of which are also correlated to the variation in bone radial location (cortical thickness).

Results

Indentation results: stiffness versus intracortical thickness

Based on the unloading portion of the force versus indentation depth profiles and on the corresponding indentation areas, longitudinal stiffness (E_{11} : Young’s modulus in the bone’s 1-direction or axial direction) values were determined. The assignment of the radial location of each indentation is based on an x - and y -coordinate system whose origin is the bone’s geometric center. For the various radial

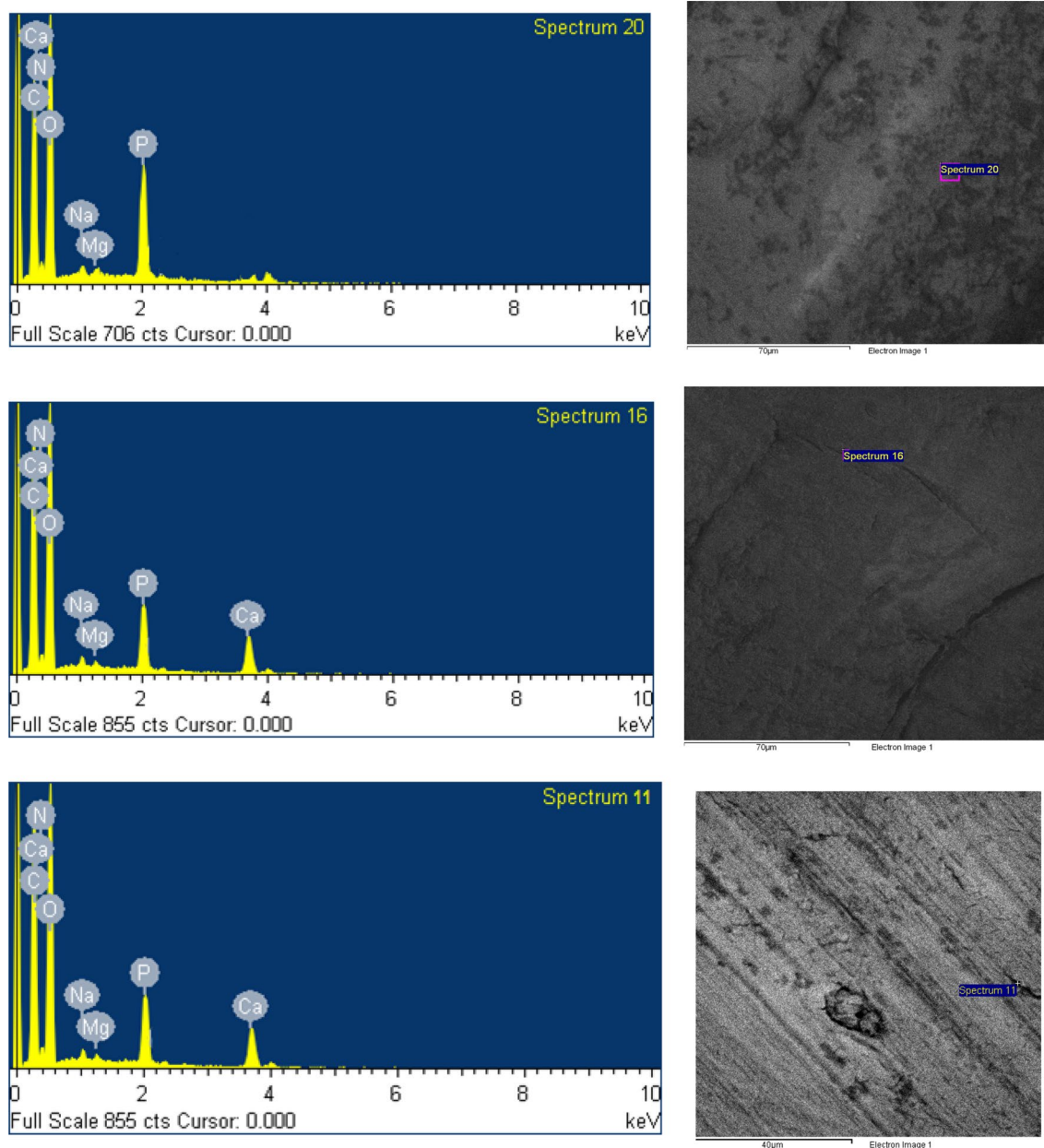


Fig. 4 Typical EDX elemental composition spectrums (left) and their corresponding SEM micrographs (right). Samples: 1 (top), 2 (middle), and 3 (bottom)

lines, the x- and y- scales reach the bone' outer cortex at distances ranging of 13.5–17.5 mm (depending on the specimen) in 0.5-mm increments (Fig. 1 (bottom-middle)). Three typical indentation force vs. penetration depth plots with loading and unloading curves are shown in Fig. 2 corresponding to 3 different bone samples dubbed samples 1 (Fig. 2a), 2 (Fig. 2b), and 3 (Fig. 2c).

Values of the modulus of elasticity were determined using the method proposed by Oliver and Pharr [29]. Indentations dimensions and areas were calculated from digital images by determining the number of pixels (Hage and Hamade

[5]). Longitudinal modulus values for bone samples 1, 2, and 3 were found to range from 18.5 to 26, 20.1–23.8, and 18–24.4 GPa, respectively. For all three bone samples, Fig. 3 shows the resulting E_{11} values plotted versus radial distance, R (intracortical thickness). Since small variations are measured in the different quadrants (Hage and Hamade [30–32]), average stiffness values are reported in Fig. 3. The found aggregate average and standard deviation stiffness modulus values are 22.34 GPa and 1.95 GPa, respectively (Luo et al. [33], Erickson et al. [34], and Cuppone et al. [22]).

Table 2 Elemental mineralization content (wt.%) and the corresponding bone radial locations

Radial location (mm)	C	N	O	Na	Mg	P	Ca
Bone 1							
13.5	20.69	3.37	33.04	2.74	0.2	12.05	27.91
14	20.33	2.56	33.1	2.56	0.19	12.43	28.83
14.5							
15	17.98	2.85	33.39	2.85	0.17	13.1	30.46
15.5							
16	22.89	2.58	25.44	2.58	0.19	14.68	31.64
16.5							
17	19.13	2.64	27.68	2.64	0.16	15.69	32.06
17.5							
Bone 2							
13.5	21.05	3.12	32.17	3.19	0.16	11.46	28.85
14	19.91	2.95	33.28	2.72	0.18	11.64	29.32
14.5							
15	20.08	3.04	30.32	3.17	0.17	12.97	30.25
15.5							
16	21.59	3.1	27.97	2.71	0.17	13.27	31.19
16.5							
17	19.36	3.17	25.62	3.26	0.19	15.23	33.17
17.5							
Bone 3							
13.5	17.31	2.57	40.52	2.04	0.16	10.58	26.82
14	18.02	2.67	35.75	2.31	0.17	12.37	28.71
14.5							
15	17.94	2.51	35.46	2	0.17	12.85	29.07
15.5							
16	15.17	2.83	34.06	1.97	0.15	14.52	31.3
16.5							
17	14.91	2.71	32.55	1.92	0.16	15.69	32.06
17.5							

Utilizing SPSS[®], equations that describe Young's modulus, E_{11} , values as function of radius, R , are developed. Table 1 lists the statistical metrics R^2 and p values for each of the three samples and for aggregated data of all three samples. All trends are found to be statistically significant (all p values < 0.05 indicating statistical significance). Pooling all samples into one dataset (last column) yields good fits of stiffness modulus versus radial location.

EDX results: mineralization versus intracortical thickness

At several locations along the same radial lines as for HV measurements (Fig. 1, bottom-right), elemental EDX spectrums were collected and analyzed. For three samples: 1 (top), 2 (middle), and 3 (bottom), Fig. 4 shows collected EDX spectrums (left) along with their corresponding SEM micrographs (right). The elements Ca, P, C, N, O, Na, and

Mg were detected in appreciable quantities. For each location and for each element detected, average elemental composition values were expressed as %wt. [35].

For the three bone samples, the average %wt. of each element was calculated for the spectrums collected at several radial locations in the range of about 13.5–17.5 mm from specimen geometric center (covering a cortical radial distance of about 4 mm). Table 2 lists the elemental mineralization wt.% along the corresponding radial locations. Mineral-content-wise, the elemental %wt. values were found to be nearly identical for the four anatomical quadrants (in agreement with Langelier et al. [35]).

Developed using SPSS[®] for all mineralization elements, Table 3 lists linear relationships between bone mineral content and bone radius, R . Checking for statistical significance, only Ca %wt., P %wt., and the ratio Ca/P were found to have strong correlations with radial location. No statistically significant linear relations were found for the other detected

Table 3 Bone mineralization versus radial location: linear trends and their statistical metrics

	Bone 1	Bone 2	Bone 3	All bones
Ca (wt.%)				
Equation	$Ca = 1.2165R + 11.811$	$Ca = 1.177R + 12.773$	$Ca = 1.4249R + 8.0763$	$Ca = 1.273R + 10.887$
<i>p</i> value	0.004	0.003	0.007	0.000
<i>R</i> ²	<i>R</i> ² =0.954	<i>R</i> ² =0.9665	<i>R</i> ² =0.9383	<i>R</i> ² =0.894
P (wt.%)				
Equation	$P = 1.068R - 2.541$	$P = 1.0296R - 2.6335$	$P = 1.3487R - 7.1627$	$P = 1.149R - 4.112$
<i>p</i> value	0.001	0.006	0.004	0.0000
<i>R</i> ²	0.972	0.942	0.985	0.913
Ca/P				
Equation	$Ca/P = -0.082R + 3.477$	$Ca/P = -0.095R + 3.816$	$Ca/P = -0.123R + 4.115$	$Ca/P = -0.1000R + 3.801$
<i>p</i> value	0.025	0.014	0.011	0.0000
<i>R</i> ²	0.854	0.898	0.915	0.713
C (wt.%)				
Equation	$C = -0.039R + 20.7888$	$C = -0.168R + 22.928$	$C = -0.894R + 30.168$	$C = 0.367R + 24.628$
<i>p</i> value	0.962	0.666	0.072	0.437
<i>R</i> ²	0.001	0.071	0.713	0.047
N (wt.%)				
Equation	$N = -0.141R + 4.927$	$N = -0.033R + 2.575$	$N = -0.048R + 1.929$	$N = -0.020R + 3.144$
<i>p</i> value	0.29	0.324	0.331	0.728
<i>R</i> ²	0.345	0.316	0.308	0.01
O (wt.%)				
Equation	$O = -2.088R + 62.065$	$O = -2.105R + 61.658$	$O = -1.845R + 63.666$	$N = -2.016R + 62.463$
<i>p</i> value	0.1	0.007	0.045	0.008
<i>R</i> ²	0.649	0.937	0.785	0.434
Na (wt.%)				
Equation	$Na = -0.018R + 2.945$	$Na = 0.027R + 2.605$	$Na = -0.071R + 3.123$	$Na = -0.021R + 2.891$
<i>p</i> value	0.731	0.82	0.219	0.828
<i>R</i> ²	0.045	0.02	0.445	0.004
Mg (wt.%)				
Equation	$Mg = -0.009R + 0.313$	$Mg = -0.005R + 0.095$	$Mg = -0.003R + 0.201$	$Mg = -0.02R + 0.203$
<i>p</i> value	0.141	0.227	0.46	0.512
<i>R</i> ²	0.569	0.434	0.192	0.034

elements: C, N, O, Na, and Mg as can be deduced from the *p* values. Therefore, Ca and P along with Ca/P ratios were retained for further consideration. Pooling mineralization content of all samples into one aggregate dataset (last column) yields good, statistically significant fits versus radial location.

CT scanning results: HU values versus intracortical thickness

The resulting CT scans of all bone samples were segmented using the software package MIMICS [27]. Figure 5 shows three such scans for samples 1 (top), 2 (middle), and 3 (bottom) with intracortical HU variations plotted along the radial

distance or cortical thickness [23]. Higher HU values are recorded at the exterior cortex (at both sides of the circumference) and decrease toward the interior regions.

For bone samples 1 (top), 2 (middle), and 3 (bottom), Fig. 6 shows experimental points and linear fits of stiffness values, calcium and phosphorus %wt. content, and HU values all co-plotted versus *R*. Similar to Fig. 3, the plotted data in Fig. 6 covers intracortical thickness ranging from about *R* = 13.5–17.5 mm (dimensions from Fig. 5 are extracted to match the dimensions in Fig. 3). All curves and fits exhibit increasing trends versus location moving from the interior to the exterior regions across the cortical thickness indicating a denser and stiffer outer cortical shell.

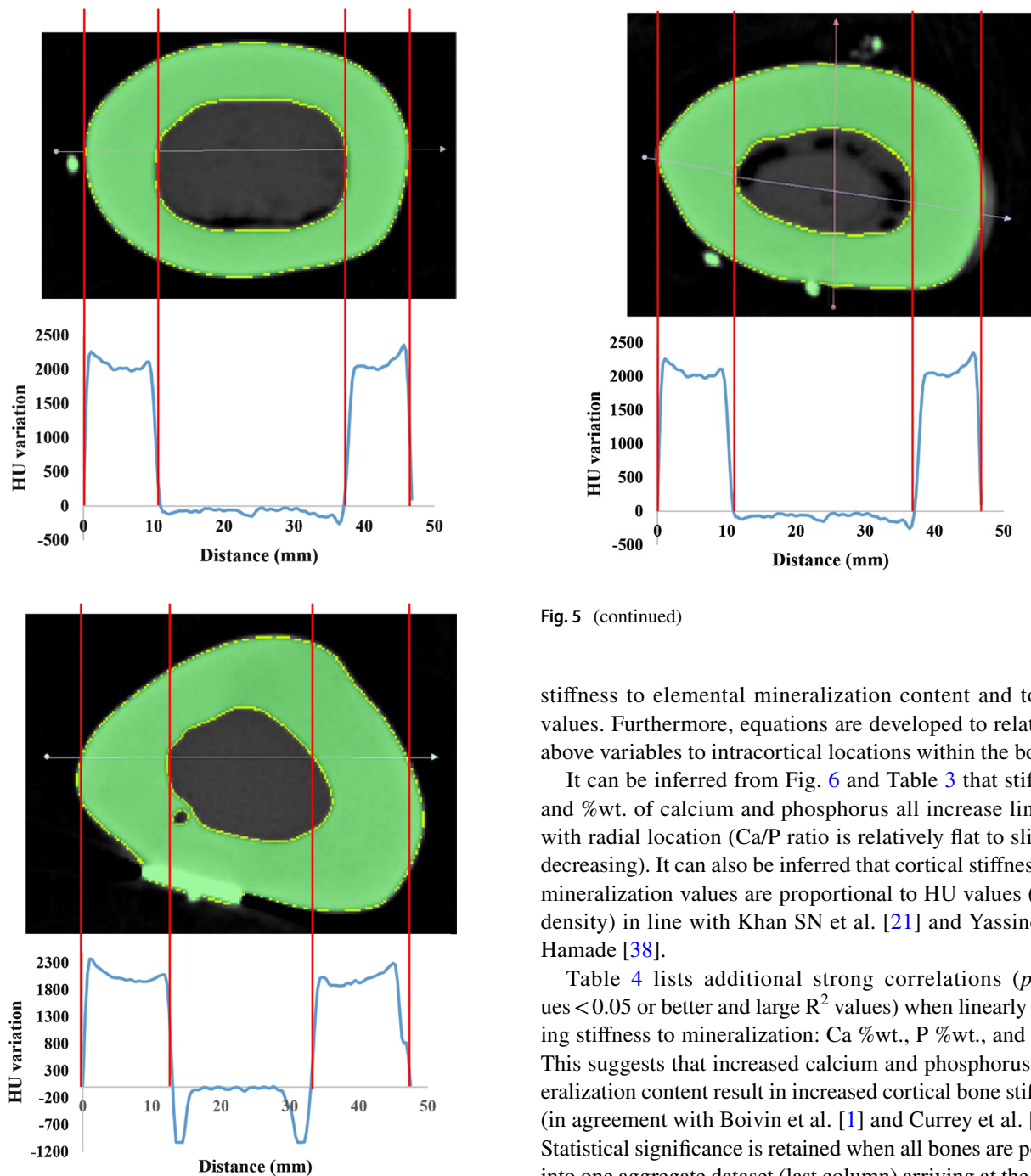


Fig. 5 CT scans showing the lines along which HU values are measured for samples: 1 (top), 2 (middle), and 3 (bottom)

Discussion

Several works (e.g., Austman et al. [36], Wirtz et al. [37]) have reported equations relating cortical bone stiffness to cortical density (or HU values). This work distinguishes itself by developing linear equations relating cortical bone

Fig. 5 (continued)

stiffness to elemental mineralization content and to HU values. Furthermore, equations are developed to relate the above variables to intracortical locations within the bone.

It can be inferred from Fig. 6 and Table 3 that stiffness and %wt. of calcium and phosphorus all increase linearly with radial location (Ca/P ratio is relatively flat to slightly decreasing). It can also be inferred that cortical stiffness and mineralization values are proportional to HU values (bone density) in line with Khan SN et al. [21] and Yassine and Hamade [38].

Table 4 lists additional strong correlations (p values < 0.05 or better and large R^2 values) when linearly relating stiffness to mineralization: Ca %wt., P %wt., and Ca/P. This suggests that increased calcium and phosphorus mineralization content result in increased cortical bone stiffness (in agreement with Boivin et al. [1] and Currey et al. [39]). Statistical significance is retained when all bones are pooled into one aggregate dataset (last column) arriving at the same conclusion reached for individual bone samples.

Table 5 lists linear equations relating bone stiffness to HU values and to intracortical location. The R^2 values listed in the table are all greater than 85% for all individual samples indicating a robust correlation between bone stiffness and HU values. This suggests that HU as a variable explains at least 85% of the variation of cortical bone stiffness with radius. HU does not appear to be statistically significant for individual bone samples 2 and 3. However, when all data are pooled together (Table 5, last column) statistical fits become

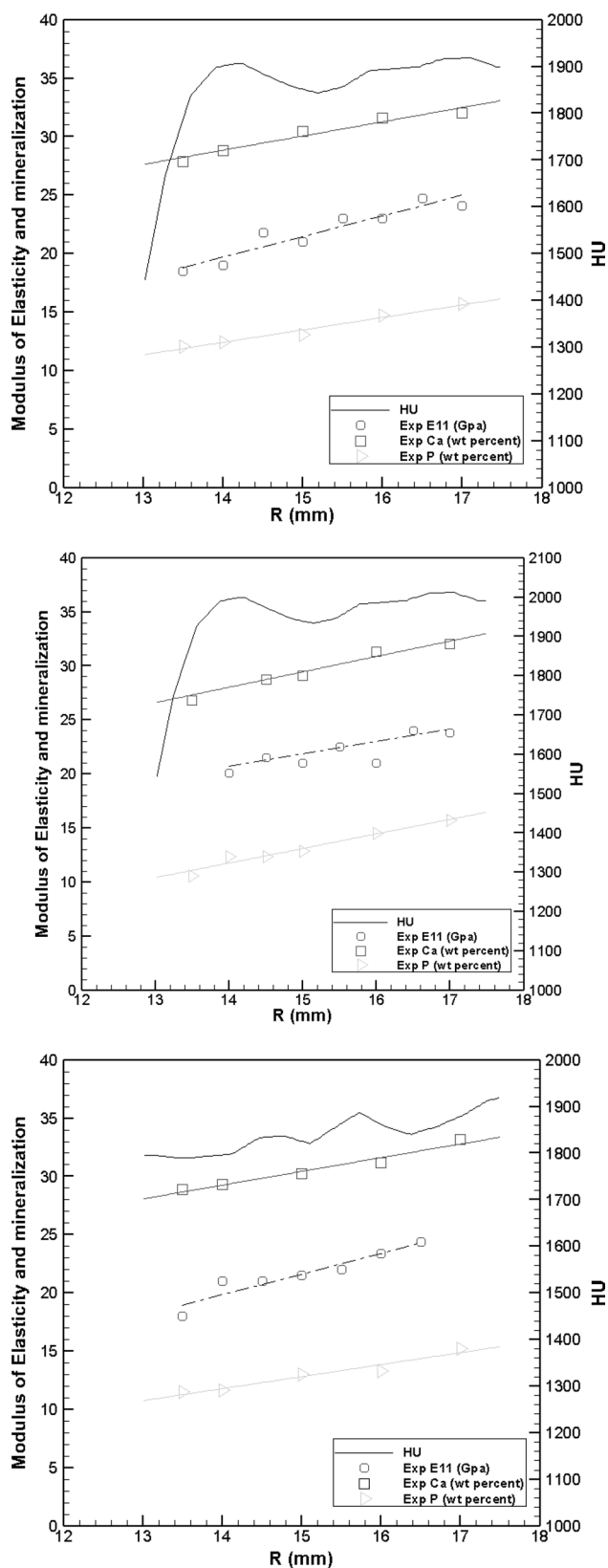


Fig. 6 Experimental points and linear fits of cortical bone modulus of elasticity values, calcium and phosphorus content, and HU values all plotted versus R for bone samples: 1 (top), 2 (middle), and 3 (bottom)

extremely significant (p values for HU and R are 0.001, and 0.000001, respectively).

Table 6 lists linear equations that correlate bone stiffness to intracortical location and to mineralization (Ca %wt. and P %wt.). Reinforcing the findings from Table 4 R^2 values in Table 6 are more significant than 84.6% for all bone samples 1, 2, and 3, again, suggesting a robust relation between bone stiffness and mineralization. It can be concluded that mineralization is a factor that greatly influences the variation of cortical bone stiffness with intracortical location. (Although Ca %wt. appears to be no longer significant when all 3 samples are pooled together, this could be an artifact presumably due to the high correlations between R , Ca, and P). The positive correlations with increasing intracortical thickness suggest increasing stiffness towards the outer cortical shell which exhibits the highest stiffness corresponding to the most significant % wt. mineralization values (in line with Franco et al. [8], Romanus [13], Langelier et al. [35]).

Last, Table 7 lists all-in-one expressions that correlate stiffness versus HU values, mineralization (Ca %wt. and P %wt.), and intracortical thickness. All variables are now combined into one equation. R^2 values are found to be 0.997 and 0.925 for bones 1 and 3 (slightly smaller R^2 value of 84.9% for bone 3). As such, cortical bone stiffness is correlatable, to HU, to mineralization and to radial location in increasing linear fashion again suggesting a stiffer and more mineralized cortical shell. (Anomalously, Ca %wt. does not appear significant when all samples are pooled together perhaps due to the statistical occurrence given the high correlations between R , Ca %wt., and P %wt.).

Summary

The main novelty of this work is the development of a mapping method that relates cortical stiffness and mineralization of cortical bone to intracortical thickness specifically the distance from the endosteal surface to the periosteal surface of mid-diaphyseal bovine femur. Stiffness-mineralization-HU interdependency equations are developed. For this purpose, cortical bone longitudinal stiffness (E_{11}), elemental mineralization content (calcium %wt. and phosphorus %wt.), and HU values are experimentally determined using Vickers indentation, EDX spectroscopy and computed tomography (CT) scans, respectively. These measurements are taken along radial lines (dubbed radial distance, R) that emanate from the geometric bone center and extend to the outer bone cortex. Results show that stiffness values exhibit increasing trends with radial distance, R , suggesting that with increasing calcium and phosphorus mineralization content, stiffness of cortical bone correspondingly increase. For further corroboration, matching and correlating trends are developed for the CT-collected HU

Table 4 Stiffness modulus vs. mineralization: linear trends and their statistical metrics

	Bone 1	Bone 2	Bone 3	All bones
E_{11} (GPa) versus Ca (wt. %)				
Equation	$E_{11} = -19.507 + 1.346Ca$	$E_{11} = -9.776 + 1.007Ca$	$E_{11} = -13.617 + 1.194Ca$	$E_{11} = -12.877 + 1.133Ca$
<i>p</i> value	0.002	0.001	0.019	0.000
R^2	0.969	0.829	0.992	0.830
E_{11} (GPa) versus P (wt. %)				
Equation	$E_{11} = -0.014 + 1.555P$	$E_{11} = 6.235 + 1.142P$	$E_{11} = 3.749 + 1.379P$	$E_{11} = 3.125 + 1.375P$
<i>p</i> value	0.002	0.005	0.008	0.0000
R^2	0.971	0.951	0.985	0.878
E_{11} (GPa) versus Ca/P				
Equation	$E_{11} = 59.934 - 17.390Ca/P$	$E_{11} = 48.814 - 11.695Ca/P$	$E_{11} = 54.002 - 14.251Ca/P$	$E_{11} = 50.134 - 12.582(Ca/P)$
<i>p</i> value	0.031	0.015	0.004	0.000
R^2	0.830	0.893	0.992	0.704

Table 5 Stiffness modulus vs. HU and R: linear trends and their statistical metrics

	Bone 1	Bone 2	Bone 3	All bones
Equation	$E_{11} = -0.83 - 0.002HU + 1.759R$	$E_{11} = -8.026 - 0.006HU + 1.087R$	$E_{11} = -0.814 - 0.004HU + 1.837R$	$E_{11} = 0.221 - 0.002HU + 1.606R$
<i>p</i> value (HU/R)	0.04/0.00001	0.313/0.00001	0.33/0.00001	0.001/0.000001
R^2	0.905	0.85	0.913	0.0855

Table 6 Stiffness modulus vs. mineralization and R: linear trends and their statistical metrics

	Bone 1	Bone 2	Bone 3	All bones
Equation	$E_{11} = -9.991 - 0.12R + 0.684Ca + 0.907P$	$E_{11} = -35.73 + 1.405R + 1.852Ca - 1.582P$	$E_{11} = -57.361 + 0.648R - 0.146Ca + 3.564P$	$E_{11} = -2.056 + 1.802R - 0.062Ca - 0.4624P$
<i>p</i> value (R/Ca/P)	0.313/0.00001/0.682	0.00001/0.00001/0.00001	0.006/0.00001/0.00001	0.0000/0.482/0.0000
R^2	0.996	0.912	0.846	0.866

Table 7 Stiffness modulus vs. mineralization, HU, and R: linear trends and their statistical metrics

	Bone 1	Bone 2	Bone 3	All bones
Equation	$E_{11} = 8.062 - 0.001HU + 0.15R + 0.611Ca + 0.76P$	$E_{11} = 74.866 - 0.008HU + 0.539R - 3.285Ca + 3.825P$	$E_{11} = -79.378 + 0.019HU + 0.616R + 2.732Ca - 2.113P$	$E_{11} = 1.750 - 0.002HU + 1.971R - 0.062Ca - 0.439P$
<i>p</i> value (HU/R/Ca/P)	0.00/0.061/0.00/0.00	0.258/0.032/0.00/0.00	0.00/0.009/0.00/0.00	0.006/0.000/0.523/0.000
R^2	0.997	0.849	0.925	0.870

values. When all data for three different bones are pooled together, statistical fits become extremely significant for the aggregate data. When tested for these correlations and combined variables, strong statistically significant correlations (as evidenced by *p* value and R^2 metrics) are found. Stiffness values are related to HU values and to calcium %wt. and phosphorus %wt. content along the radial distance. Thanks to higher mineralization, these

findings suggest that the cortex possesses higher stiffness and density than inner regions. The predictive capabilities of these developed linear equations of femur cortical bone stiffness in relation to mineralization and HU values may help medical researchers reduce invasive methods when characterization of bones is desirable.

Acknowledgements This work was made possible by the financial support of the Lebanese National Council for Scientific Research (CNRS) Award Number 103087. The authors also acknowledge the support of the University Research Boards (URB) of the American University of Beirut and the Notre Dame University-Louaize for their financial aid of this work.

Author contributions ISH, RSH, RAY and CYS contributed to research studies, analysis and writing. RFH supervised the work and contributed to reviewing and editing the work.

References

- Boivin G, Bala Y, Doublier A, Farlay D, Ste-Marie LG, Meunier PJ, Delmas PD (2008) The role of mineralization and organic matrix in the microhardness of bone tissue from controls and osteoporotic patients. *Bone* 43:532–538
- Bala Y, Depalle B, Douillard T, Meille S, Clément P et al (2011) Respective roles of organic and mineral components of human cortical bone matrix in micromechanical behavior: an instrumented indentation study. *J Mech Behav Biomed Mater* 4:1473–1482
- Haider IT, Lobos SM, Simonian N, Schnitzer TJ, Edwards WB (2018) Bone fragility after spinal cord injury: reductions in stiffness and bone mineral at the distal femur and proximal tibia as a function of time. *Osteop Int* 29:2703–2715
- Cai X, Follet H, Peralta L, Gardegaront M, Farlay D et al (2019) Anisotropic elastic properties of human femoral cortical bone and relationships with composition and microstructure in elderly. *Acta Biomater* 90:254–266
- Hage IS, Hamade RF (2017) Intracortical Stiffness of Mid-Diaphysis Femur Bovine Bone: Lacunar–canalicular Based Homogenization Numerical Solutions and Microhardness Measurements. *J Mater. Sci Mater Med* 28(9):135–147
- Boskey AL, Posner AS (2018) Structure and formation of bone mineral. In: Hastings GW, Ducheyne P (eds) *Natural and living biomaterials*. CRC Press Boca Raton, Florida, pp 27–41
- Bonfield W (2018) Elasticity and viscoelasticity of cortical bone. In: Hastings GW, Ducheyne P (eds) *Natural and living biomaterials*. CRC Press, Boca Raton, Florida, pp 43–60
- Franco GL, Blank RD, Akhter MP (2011) Intrinsic material properties of cortical bone. *J bone min meta* 29:31–36
- Boivin G, Meunier PJ (2002) The degree of mineralization of bone tissue measured by computerized quantitative contact microradiography. *Calcif Tissue Int* 70:503–511
- Follet H, Boivin G, Rumelhart C, Meunier PJ (2004) The degree of mineralization is a determinant of bone strength: a study on human calcanei. *Bone* 34:783–789
- Boivin GY, Chavassieux PM, Santora AC, Yates J, Meunier PJ (2000) Alendronate increases bone strength by increasing the mean degree of mineralization of bone tissue in osteoporotic women. *Bone* 27:687–694
- Hansson T, Roos B, Nachemson ALF (1980) The bone mineral content and ultimate compressive strength of lumbar vertebrae. *Spine (Phila. Pa. 1976)* 5:46–55
- Romanus B (1974) Physical properties and chemical content of canine femoral cortical bone in nutritional osteopenia: its reversibility and the effect of fluoride. *Acta Orthop Scand Suppl* 155:1–101
- Zaichick V, Tzaphlidou M (2003) Calcium and phosphorus concentrations and the calcium/phosphorus ratio in trabecular bone from the femoral neck of healthy humans as determined by neutron activation analysis. *Appl Radiat Isot* 58:623–627
- Tzaphlidou M, Speller R, Royle G, Griffiths J, Olivo A, Pani S, Longo R (2005) High resolution Ca/P maps of bone architecture in 3D synchrotron radiation microtomographic images. *Appl Radiat Isot* 62:569–575
- Tzaphlidou M (2008) Bone architecture: collagen structure and calcium/phosphorus maps. *J Bio Phys* 34:39–49
- Mandair GS, Morris MD (2015) Contributions of Raman spectroscopy to the understanding of bone strength. *BoneKEY reports*, p 4
- Willems NMBK, Mulder L, den Toonder JMJ et al (2014) The correlation between mineralization degree and bone tissue stiffness in the porcine mandibular condyle. *J Bone Miner Metab* 32:29–37
- Huang HL, Tsai MT, Lin DJ, Chien CS, Hsu JT (2010) A new method to evaluate the elastic modulus of cortical bone by using combined computed tomography and finite element approach. *Biol Med* 40:464–468
- Yang G, Kabel J, VanRietbergen B, Odgaard A, Huiskes R, Cowin S (1999) The anisotropic Hooke's law for cancellous bone and wood. *J Elast* 53:125–146
- Rho JY, Hobatho MC, Ashman RB (1995) Relations of mechanical properties to density and CT numbers in human bone. *Med Eng Phys* 17:347–355
- Cuppone M, Seedhom BB, Berry E, Ostell AE (2004) The longitudinal Young's modulus of cortical bone in the midshaft of human femur and its correlation with CT scanning data. *Calcif Tissue Int* 74(3):302–309
- Schneider R, Faust G, Hindenlang U, Helwig P (2009) Inhomogeneous, orthotropic material model for the cortical structure of long bones modelled on the basis of clinical CT or density data. *Comp Meth Appl Mech Eng* 198:2167–2174
- Khan SN, Warkhedkar RM, Shyam AK (2014) Analysis of Hounsfield unit of human bones for strength evaluation. *Proc mat sci* 6:512–519
- Eberle S, Göttlinger M, Augat P (2013) An investigation to determine if a single validated density-elasticity relationship can be used for subject specific finite element analyses of human long bones. *Med Eng Phys* 35:875–883
- Gačnik F, Ren Z, Hren NI (2014) Modified bone density-dependent orthotropic material model of human mandibular bone. *Med Eng Phys* 36:1684–1692
- Mimics student edition course book, Innovation Suite Research, Materialize Technologielaan 15–3001 Leuven-Belgium, <http://www.materialise.com/en/medical/software/mimics>, Accessed 10 Jan 2017
- Yassine RA, Elham MK, Mustapha S, Hamade RF (2017) A detailed methodology for FEM analysis of long bones from CT using Mimics. In: *ASME International Mechanical Engineering Congress and Exposition 2017 Nov 3* (Vol. 58363, p. V003T04A012). American Society of Mechanical Engineers.
- Oliver WC, Pharr GM (2004) Measurement of hardness and elastic modulus by instrumented indentation: Advances in understanding and refinements to methodology. *J Mat Res* 19:3–20
- Hage IS, Hamade RF (2015) Distribution of porosity in cortical (Bovine) Bone. In: *Paper No. IMECE2015–51703*, pp. V003T03A085; *ASME 2015 International Mechanical Engineering specimen Congress and Exposition, Volume 3: Biomedical and Biotechnology Engineering specimen*, Houston, Texas, USA, November 13–19, 2015.
- Hage IS, Hamade RF (2016) Geometric-attributes-based segmentation of cortical bone slides using optimized neural networks. *J Bone Miner Metab* 34:251–265
- Hage IS, Hamade RF (2018) Relating bone intra-cortical elastic stiffness to EDX spectroscopy mineralization measurements. In: *Paper No. IMECE2018–86233; ASME 2018 International Mechanical Engineering Congress and Exposition, Volume 3:*

- Biomedical and Biotechnology Engineering, Pittsburgh, USA, November 9–15, 2018
33. Luo C, Liao J, Zhu Z, Wang X, Lin X, Huang W (2019) Analysis of mechanical properties and mechanical anisotropy in canine bone tissues of various ages. *BioMed Res Int* 2019:3503152
 34. Erickson GM, Catanese J III, Keaveny TM (2002) Evolution of the biomechanical material properties of the femur. *Anat Rec* 268:115–124
 35. Langelier B, Wang X, Grandfield K (2016) Atomic scale chemical tomography of human bone. *Sci Rep* 7:1–9
 36. Austman RL, Milner JS, Holdsworth DW, Dunning CE (2009) Development of a customized density—modulus relationship for use in subject-specific finite element models of the ulna. *Proc Inst Mech Eng Part H J Eng Med* 223:787–794
 37. Wirtz DC, Schiffers N, Pandorf T, Radermacher K, Weichert D, Forst R (2000) Critical evaluation of known bone material properties to realize anisotropic FE-simulation of the proximal femur. *J Biomech* 33:1325–1330
 38. Yassine RA, Hamade RF (2019) Transversely isotropic and isotropic material considerations in determining the mechanical response of geometrically accurate bovine tibia bone. *Med Bio Eng Comp* 57(10):2159–2178
 39. Currey JD, Brear K, Zioupos P (1996) The effects of ageing and changes in mineral content in degrading the toughness of human femora. *J Biomech* 29:257–260

Publisher's Note Springer Nature remains neutral with regard to jurisdictional claims in published maps and institutional affiliations.